RESEARCH ARTICLE | FEBRUARY 06 2025

First-principles study on segregation anisotropy of grain boundaries in Pt–Au alloys

Xin Yao ; Ya-Fang Guo ; Wei Li; Kalevi Kokko ; Changle Li; Levente Vitos

J. Appl. Phys. 137, 055107 (2025)
https://doi.org/10.1063/5.0238622

Journal of Applied Physics ARTICLE pubs.aip.org/aip/jap

First-principles study on segregation anisotropy of grain boundaries in Pt–Au alloys

Cite as: J. Appl. Phys. **137**, 055107 (2025); doi: 10.1063/5.0238622
Submitted: 13 September 2024 · Accepted: 19 January 2025 ·
Published Online: 6 February 2025

Xin Yao,[1,2] Ya-Fang Guo,[1,a)] Wei Li,[3] Kalevi Kokko,[4] Changle Li,[3] and Levente Vitos[3,5,a)]

AFFILIATIONS

[1]Department of Mechanics, School of Physical Science and Engineering, Beijing Jiaotong University, Beijing 100044, China
[2]State Key Laboratory of Advanced Technologies for Comprehensive Utilization of Platinum Metals, Kunming Institute of Precious Metals, Kunming 650106, China
[3]Applied Materials Physics, Department of Materials Science and Engineering, KTH Royal Institute of Technology, SE-10044 Stockholm, Sweden
[4]Department of Physics and Astronomy, University of Turku, FIN-20014 Turku, Finland
[5]Department of Physics and Astronomy, Division of Materials Theory, Uppsala University, Box 516, SE-75120 Uppsala, Sweden

[a)]**Authors to whom correspondence should be addressed:** yfguo@bjtu.edu.cn and leveute@kth.se

ABSTRACT

Gold (Au) segregation at Pt grain boundaries (GBs) plays an important role in the properties of Pt-based alloys. It was reported that close-packed GBs and open GBs exhibit different segregation behaviors, and their origin is still unclear. Based on the density functional theory as implemented in the exact muffin-tin orbitals method and the full charge density technique, we investigate the impact of bulk composition and temperature on the segregation behaviors of the $\Sigma3(111)[1\bar{1}0]$, $\Sigma5(310)[001]$, and $\Sigma9(221)[1\bar{1}0]$ symmetric tilt GBs in Pt–Au alloys. It is revealed that the segregation driving forces are correlated with the large local volume near the GB and the miscibility gap in Pt–Au alloys. At finite temperatures when the configurational entropy is considered, a competition between the chemical driving force and the configurational entropy is responsible for the segregation anisotropy in Pt–Au alloys. The bulk composition has a small effect on the segregation energy but strongly impacts the equilibrium concentration profiles at finite temperatures. The present study provides a theoretical analysis for the segregation anisotropy, and the methodology utilized in this work can be generalized to other binary or multi-component dilute or concentrated alloys while the composition variation is involved.

I. INTRODUCTION

Platinum (Pt) has superior oxidation and corrosion resistance and is commonly used as electrical contacts,[1] rocket propulsion nozzles,[2] thermocouples,[3,4] and electrocatalysts.[5–7] Its price has always been the biggest obstacle in the development of Pt applications, but its excellent performance makes it challenging to find suitable alternatives. For instance, in electrocatalysis of the oxygen reduction reaction (ORR) and hydrogen evolution reaction (HER) in acidic media, no other metal can compete with Pt.[8] Considering the price and criticality of Pt, it is of great significance to improve the utilization efficiency of Pt. One effective way to strengthen a metal is to add alloying elements. Gold (Au) is of particular interest because of its prominent role in improving the properties of Pt. Several studies showed that Au can improve the hardness and strength of Pt.[3,9] Curry *et al.*[1] reported that the $Pt_{0.90}Au_{0.10}$ alloy has extraordinary resistance to wear. Lu *et al.*[10] demonstrated that $Pt_{0.90}Au_{0.10}$ exhibits remarkable stability compared to that of pure Pt films processed under identical conditions. Because of the inertness of Au in the bulk state and its high catalytic activity at the nanoscale, Au is also added to Pt to improve the catalytic properties.[7] The Pt–Au combination has been proven to be beneficial, performing better than Pt alone in the oxygen reduction of the fuel cell cathode.[11]

The enhanced properties of the Pt–Au alloy are mainly attributed to preferential Au segregation.[8,10] Therefore, it is rewarding to understand the fundamentals of the atomic-level mechanisms behind the segregation in Pt–Au alloys. Experimental studies of the

segregation have been carried out using a scanning transmission electron microscope (STEM), three-dimensional atom probe tomography (3D APT), and energy-dispersive x-ray spectroscopy (EDS).[12,13] Curry *et al.*[1] measured the Au distribution in $Pt_{0.90}Au_{0.10}$ films with STEM-EDS. After annealing at 773 K, Au enrichment at Pt grain boundaries (GBs) and free surfaces with highly heterogeneous distributions was observed. Lu *et al.*[10] investigated pure Pt and $Pt_{0.90}Au_{0.10}$ alloy films with two thicknesses by annealing them at 773 and 973 K. STEM and x-ray diffraction (XRD) measurements demonstrated that Au segregation to Pt GBs is heterogeneous and varies in solute content between different GBs. However, heterogeneous segregation is reduced as the temperature increases from 773 to 973 K. Moreover, low-energy GBs, e.g., closed-packed twin boundaries, do not show Au enrichment, but substantial Au segregation is observed at high-energy (open) GBs. Zhou *et al.*[8] found that after an annealing treatment at 773 K for 100 h, Au segregation is readily observed in Pt–5 at. % Au thin films. The STEM measurements showed that Au segregates at low-angle GBs, high-angle GBs, Σ3-type, Σ7-type, and other coincidence site lattice (CSL) GBs, where Σ is the density of the coincident sites. Barr *et al.*[14] reported that after thermal annealing of Pt–10 at. %Au at 773 K for 30 min, Au concentration reached 30–43 at. % at high-angle GBs and 17–22 at. % at low-angle GBs, while no Au segregation was detected on a closed-packed Σ3(111) twin boundary. The above experimental results indicate that the Au segregation to Pt GBs is heterogeneous and varies with the annealing temperature and the type of the GBs.

Computational simulations are powerful tools for segregation studies. Up to date, only limited theoretical investigations deal with Au segregation at Pt GBs, and most works focused on the influence of GB character on the solute concentration, e.g., the misorientation effect of GBs. In earlier years, Foiles and his colleagues did a series of segregation studies for Au–1 at. % Pt and Pt–1 at. % Au alloys with Monte Carlo simulations based on embedded atom method (EAM) potentials.[15–19] They examined the structural and temperature effects on solute-atom segregation at [001] twist GBs and Σ5(310) tilt GB and found that the solute atom is enhanced at GBs on the Pt-rich side of the phase diagram and is depleted on the Au-rich side. At low temperatures, the segregation tendency increases monotonically as twist angle θ increases up to about 35°, while the dependence of segregation on the GB structure is weak at high temperatures. Barr *et al.*[14] explored the GB solute segregation and its dependency on GB misorientation in nanocrystalline Pt–10 at. % Au alloy systems by atomistic simulations. It was found that GB misorientation has a significant effect on the segregation of Au at Pt GBs. GB concentration profiles and resultant segregation energies could vary up to a factor of 3 with GB misorientation. Furthermore, the Σ3(111) twin boundary exhibits no Au segregation due to zero segregation energy. Through atomistic simulations using Large-scale Atomic/Molecular Massively Parallel Simulator (LAMMPS), Priedeman and Thompson[20] studied the segregation behavior of a Σ21*a* ([111] 21.8°) tilt GB (where Σ21 is the density of the coincident sites and *a* is a GB variant). They found that the preferential Au segregation reduces the GB energy and, thus, stabilizes the GB facet. O'Brien *et al.*[21] demonstrated the inhomogeneity in the degree of GB segregation in Pt–10 at. % Au alloys by using molecular dynamics simulations. They revealed that the GB structure can modify the degree of segregation, and they predicted the existence of a GB phase transformation between low and high solute content GBs.

The above-mentioned experimental and computational studies on the segregation of Au at Pt GBs were limited to fixed bulk compositions, and the dependence of segregation on the bulk composition has not been considered. Accurate treatment of real materials requires a detailed understanding of segregation phenomena throughout the compositional space, especially in concentrated alloy systems. This is critical because traditional models based on dilute-solution approximations, which neglect solute–solute interactions, may fail to accurately describe the segregation behavior. For example, the spontaneous GB roughening observed in high entropy alloys is caused by the complex interplay of multiple solute elements at high concentrations, and this roughening will further affect GB energy and GB migration, leading to a different behavior from the dilute system.[22] Scheiber *et al.*[23] studied GB segregation and cohesion in W–25 at. % Re alloys and found that dilute limit approximations overestimate the segregation energies (up to 15% for high-energy GBs and about 5% for the low-energy GBs). Wagih and Schuh[24] pointed out that accurate prediction of segregation beyond the dilute limit requires consideration of both the spectrality of GB sites and solute–solute interactions. Considering the limitations of the dilute-solution models, a generalizable model, applicable to both dilute and concentrated alloys, is needed to fully understand the segregation behavior in Pt–Au alloys.

In addition, all the above-mentioned theoretical studies on Au segregation at Pt GBs are based on the simulations adopting semi-empirical potentials. Calculations based on density functional theory (DFT) are generally expected to be more reliable than semi-empirical atomic simulations due to their first-principles character, i.e., no empirical parameters. Nowadays, DFT calculations have been successfully applied to the study of GB structure and GB segregation in dilute and concentrated alloy systems.[23,25–28] Therefore, here, we adopt DFT in combination with alloy theory to systematically investigate the bulk composition and temperature dependence of the GB segregation in Pt–Au alloys. We focus on three symmetric tilt GBs, one is a close-packed Σ3(111)[1$\bar{1}$0] GB, and the other two GBs are Σ5(310)[001] and Σ9(221)[1$\bar{1}$0], which are commonly observed in fcc metals. In the following notations of the GBs, we omit the rotation axis for convenience. The latter two GBs have a smaller atomic density per unit GB area and a more open structure than the Σ3(111) GB. Therefore, by comparing the segregation behavior of these three GBs, we can reveal and analyze their segregation mechanisms and anisotropy.

The structure of the work is as follows. In Sec. II, we present the methodological details and assess the accuracy of our approximations by studying the bulk phase diagram as a fundamental descriptor for alloys. In Sec. III, we present the results. First, the static (0 K) segregation energies of the three tilt GBs in $Pt_{1-c}Au_c$ (c is the Au bulk concentration) systems are presented. Next, we put forward the theoretical segregation profiles at finite temperatures. In Sec. IV, the driving force for segregation is revealed, and the reason for segregation anisotropy is discussed.

II. METHODOLOGY

A. GB energy and the segregation energy

GB energy is the key thermodynamic quantity used to characterize the GBs. At 0 K, it is defined as an excess energy relative to

the pristine bulk system, viz.,

$$\gamma_{gb} = (E_{gb} - nE)/2A, \tag{1}$$

where E_{gb} is the total energy of the supercell with two GBs, E is the energy per atom of the bulk system, n is the number of atoms in the supercell, A is the area of the GB, and the factor of 2 stands for the two identical GBs in the supercell (due to the periodic boundary conditions). The bulk energy is calculated using the standard fcc unit cell.

The GB segregation energy is defined as the energy difference of a solute atom being situated at a GB site or in the bulk. In terms of chemical potentials, the segregation energy for GB sites i can be expressed as

$$E^i_{\text{seg}} = \Delta\mu^{gb}_i(c, \{c_i\}) - \Delta\mu^B(c), \tag{2}$$

where $\Delta\mu^{gb}_i$ is the effective chemical potential (ECP) for the GB sites i, and $\Delta\mu^B$ is the bulk ECP. ECPs are defined as the difference between the Au and Pt chemical potentials. Here, we use two methods to calculate the GB and bulk ECP. For exact muffin-tin orbitals method (EMTO) calculations, within the alloy formalism, the ECPs can be calculated from the concentration derivative of the total energies taken at a constant volume, viz.,

$$\Delta\mu^B(c) = dE(c)/dc, \tag{3}$$

$$\Delta\mu^{gb}_i(c, \{c_i\}) = dE_{gb}(c, \{c_i\})/dc_i, \tag{4}$$

where $dE(c)$ is the change of the total energy of the bulk unit cell corresponding to the concentration variation $dc = 0.01$, and $dE_{gb}(c, \{c_i\})$ is the change of the total energy of the GB supercell for a concentration variation of dc_i =0.01 (all other concentrations are kept constant). Here, $\{c_i\} = c_1, c_2, \ldots, c_i, \ldots, c_N$ are the solute concentrations at the GB sites, and N stands for the number of GB sites included in the segregation study.

For Vienna *Ab initio* Simulation Package (VASP) calculations, ECPs are calculated as the energy difference between a solute-doped system and a pure system, namely, $\Delta\mu^{gb}_i = \frac{E^{gb}_i(\text{solute}) - E_{gb}(\text{pure})}{M}$, and $\Delta\mu^B = \frac{E(\text{solute}) - E(\text{pure})}{M}$, where M denotes the number of solute atoms included in the GB and bulk supercells. Here, we used one solute atom to substitute a matrix atom, so $M = 1$. The bulk supercell consists of a $2 \times 2 \times 2$ fcc unit cell; this cell size is sufficient to obtain the accurate bulk ECP, with an error of about 0.4%.

The above-defined ECPs are computed at 0 K and, thus, the segregation energy in Eq. (2) describes the segregation behavior at 0 K. Further details of the ECP calculations are given in the supplementary material.

B. Temperature effect

The GB segregation profile at temperature T can be obtained by considering the Gibbs energy instead of the internal energy in the above formulas. In the present application, the Gibbs energy at temperature T is approximated by the internal energy plus the configurational entropy term. We neglect all other thermal effects (lattice vibrations, lattice expansion, electron excitations), as well as the possible local lattice distortion and ordering effects. The validity of this approximation in the case of the Pt–Au system will be assessed in Sec. II D.

For the segregation study at finite temperature, we follow the procedure from Ref. 29, where instead of computing the temperature-dependent ECPs, one uses the ECPs at 0 K and the configurational entropy contribution is included analytically. The GB segregation profile can be determined as a function of the bulk concentration c and temperature T by minimizing the total Gibbs energy,

$$\begin{aligned} G^{tot}(\{c_i\}) - G^{tot}(c) = E_{gb}(c, \{c_i\}) - \left\{\Delta\mu^B(c) + k_B T[lnc - \ln(1-c)]\right\} \\ \times \sum_i^N (c - c_i) + k_B T \\ \times \sum_i^N [c_i lnc_i + (1 - c_i) ln(1 - c_i)], \end{aligned} \tag{5}$$

in terms of solute concentrations $\{c_i\}$. Here, k_B is the Boltzmann constant. The internal energy of the supercell $E_{gb}(c, \{c_i\})$ is obtained from GB calculations and corresponds to GB concentrations $\{c_i\}$ and bulk concentration c. In Eq. (5), the summations run over the GB lattice sites considered in the segregation study. In practice, N is limited only by the computational time. Note that the configurational entropy considered here accounts, within the mean-field approximation, for the entropy associated with the substitutional randomness within the lattice planes parallel to the GB. However, the disorder caused by the complexity of the GB structure is neglected.

C. Computational details

The present total energy calculations are based on DFT as implemented in the exact muffin-tin orbitals method (EMTO) and the full charge density technique.[30,31] The EMTO Green function was calculated for 16 complex energy points distributed exponentially on a semicircular contour including the valence states. The muffin-tin basis sets included s, p, d, and f orbitals. The exchange-correlation functional was described using the generalized gradient approximation parameterized by Perdew–Burke–Ernzerhof (PBE).[32] The compositional disorder was treated via coherent potential approximation (CPA).[33,34] A uniform k-mesh of $29 \times 29 \times 29$ was used for the lattice parameter calculations at 0 K.

To determine the input GB structures used in EMTO, calculations based on the Vienna *Ab initio* Simulation Package (VASP) software[35] were also performed. These additional calculations also enabled a comparison between the EMTO and VASP results for dilute alloys. For the VASP calculations, PBE was adopted to describe the exchange-correlation functional, and the projector–augmented–wave (PAW) method was used for the electron–ion interactions.[36] The energy cutoff was set as 450 eV, and self-consistent convergence accuracy was selected to be 10^{-4} eV. A k-mesh of $15 \times 15 \times 15$ was used to calculate the VASP lattice constants at 0 K. Subsequently, three symmetric tilt GBs were constructed based on the obtained lattice constants of Pt and Au. According to the CSL theory, the GB structures were created by rotating one grain relative

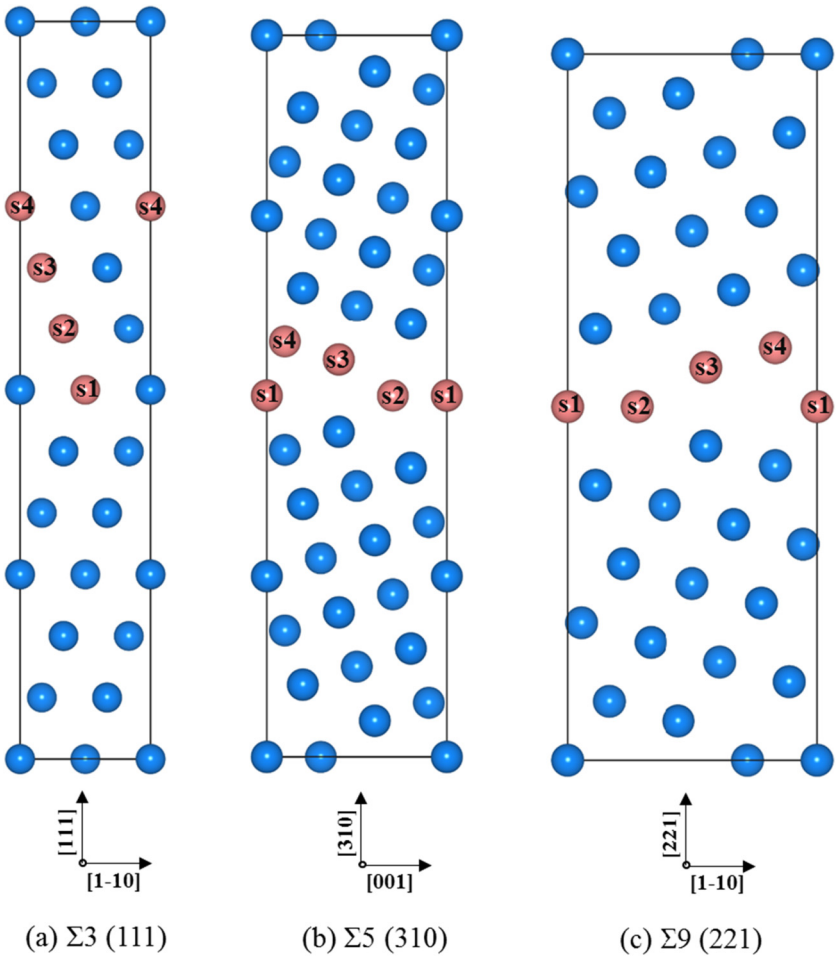

FIG. 1. Schematics of the three GB structures considered here. The blue circles represent the matrix atoms (solvent), and the pink circles represent the positions that were substituted one-by-one by the solute atoms. These four independent GB sites (indicated by 1, 2, 3, 4) are chosen to calculate the segregation energies.

to the other grain over an angle (θ) about their common [1$\bar{1}$0] or [001] tilt axis. The initial GBs were generated following the steps described in the literature,[37] where atoms at the interface that are less than 70% of the bulk interatomic distance are merged and with no basal plane translations. The ground state structures of the three GBs were then obtained by relaxing the atom positions and dimensions perpendicular to the GB plane, while the dimensions parallel to the GB plane remained unchanged. Structural relaxation was stopped when the forces acting on atoms were less than 0.01 eV/Å. It should be noted that GBs can exist in multiple states or phases and exhibit first-order transitions. Therefore, prediction of the GB structures requires sampling of many possible configurations.[38] In other words, grand-canonical evolutionary search is necessary to predict the ground state and possible multiple phases of GBs, but it is beyond the scope of our study.

The schematics of the three GBs are shown in Fig. 1. Details regarding GB dimensions are presented in Table I. Periodic boundary conditions are applied here; so, the supercell models include two identical GBs. The Σ3(111), Σ5(310), and Σ9(221) GB supercells contain 24, 38, and 34 atoms, respectively. Tests of the supercell dimensions are shown in Fig. S2 in the supplementary material. The results show that increasing the size normal to the GB plane has a small effect on the GB energy, the error is within 0.03 J/m^2, which is acceptable for our findings, and our GB energies are consistent with the literature data.[37,39,40] In addition, we test the effect of supercell size on the segregation energy. The data in Fig. S3 in the supplementary material show that our models of the Σ5(310) and Σ9(221) GBs are sufficient to obtain converged segregation energies. In contrast, for the Σ3(111) GB, we observed a non-negligible size

TABLE I. The GBs considered in this work. Listed are the tilt angles, number of atoms in the supercell, and the k-meshes for the Brillouin zone integration in both VASP and EMTO calculations.

GBs	Angle (θ)	Atoms	*k*-mesh
Σ3(111)	109.47°	24	19 × 11 × 2
Σ5(310)	53.13°	38	12 × 7 × 2
Σ9(221)	38.94°	34	17 × 5 × 2

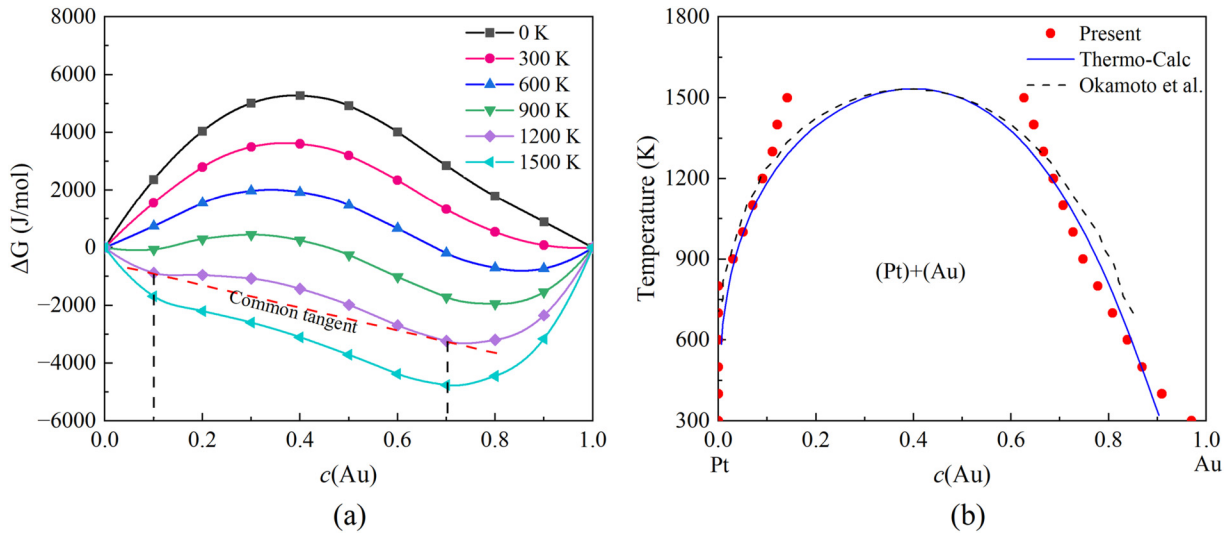

FIG. 2. (a) Gibbs energy of $Pt_{1-c}Au_c$ alloys at different temperatures; the black dotted line illustrates the solubility limits at 1200 K. (b) Theoretical bulk phase diagram. The experimental values (Okamoto and Massalski)[44] and the thermodynamic (Thermo-Calc) results[45] are presented for comparison.

effect arising from the interaction of solute atoms with their periodic images, indicating that larger models are needed to achieve convergence. However, this size effect is not significant for the overall trend since the segregation energy of Au at Σ3(111) is very small. Given the substantial computational costs required for the subsequent ECP calculations, we chose the small GB models.

The VASP calculations predicted lattice parameters of 3.968 Å for fcc Pt and 4.157 Å for fcc Au. In the EMTO calculations, the predicted lattice parameters are 3.987 Å for fcc Pt and 4.174 Å for fcc Au. Thus, the EMTO lattice parameters are slightly larger than the VASP results, but the differences are within the typical errors associated with such calculations, namely, 0.48% for fcc Pt and 0.41% for fcc Au. Both VASP and EMTO results are in line with the previous DFT calculations.[41–43] We note that when the VASP-relaxed GB structure was used as the input structure for the EMTO calculations, the GB dimensions were rescaled (keeping internal positions rigid) according to the bulk lattice parameters of fcc Pt and fcc Au determined by EMTO. This decreases the discrepancy between the VASP and EMTO calculations because no additional structural relaxations were considered in the EMTO studies.

Since the difference in lattice parameters calculated by VASP and EMTO was small, the EMTO calculations used the same k-mesh as the VASP calculations in the GB calculations. After the convergence test (as shown in Fig. S1 in the supplementary material), appropriate k-meshes were adopted for the three GB structures. These are listed in Table I.

D. Assessing the accuracy in the case of bulk Pt–Au alloys

In this section, we assess the accuracy of our approach in the case of bulk Pt–Au alloys. For a reliable GB study, the total energies and the corresponding Gibbs energies with all employed approximations should be suitable to describe the bulk phase diagram of the binary system. We consider this a necessary condition for any further segregation studies. According to the adopted approximations, the Gibbs energy of mixing at temperature T is

$$\Delta G = E(Pt_{1-c}Au_c) - (1-c)E(Pt) - cE(Au) - TS_{conf}, \quad (6)$$

where $E(Pt_{1-c}Au_c)$ is the total energy of the alloy systems, $E(Pt)$ and $E(Au)$ are the total energies of the alloy constituents in their ground states, c is the Au concentration, T is temperature, and S_{conf} is the configurational entropy.

We computed the Gibbs energies for a series of temperatures (from 0 to 1500 K with a step of 300 K) and compositions (from 0% to 100% with a step of 10%). In these calculations, the theoretical static equilibrium volumes were adopted at all temperatures. From the Gibbs energies vs composition calculated at each temperature [Fig. 2(a)], we estimated the bulk phase diagram of the Pt–Au alloy. The predicted phase diagram as a function of temperature and concentration is shown in Fig. 2(b). The experimental[44] and thermodynamic[45] phase boundaries are also shown for comparison. It can be seen that the present theoretical solubility limits are in good agreement with the experimental data and the Thermo-Calc results for temperatures below ~1300 K, but they deviate strongly at higher temperatures. We recall that in the present approximation, only the internal energy and the configurational entropy are taken into account in Gibbs energy, and all calculations correspond to the static equilibrium volumes. In other words, the effect of thermal expansion and, thus, the anharmonic effect in Gibbs energy is neglected. This is a reasonable approximation because at low temperatures, the anharmonic effects are small. As the temperature increases, they contribute more to the decrease in Gibbs energy. Since the magnitude of anharmonicity is roughly related to

the excess volume of GBs, open GBs are more susceptible to anharmonic effects than close-packed GBs.[46] Nonetheless, we assume in our work that the anharmonic effect in Gibbs energy is still small in the temperature range (below 1300 K), which is supported by the calculated phase diagrams. Therefore, we perform all GB segregation studies below 1300 K using the approximate Gibbs energy from Eq. (5).

According to the bulk phase diagram, we selected seven compositions, $Pt_{0.99}Au_{0.01}$, $Pt_{0.90}Au_{0.10}$, $Pt_{0.80}Au_{0.20}$, $Pt_{0.30}Au_{0.70}$, $Pt_{0.20}Au_{0.80}$, $Pt_{0.10}Au_{0.90}$, and $Pt_{0.01}Au_{0.99}$, for the GB studies. The reason for selecting three Pt-rich and four Au-rich alloys is the asymmetry of the bulk phase diagram. The first three compositions model the Pt-rich side of the phase diagram while the last four compositions model the Au-rich side. The primary aim is to investigate the Pt-rich alloys and, therefore, most of the results will be shown and discussed for the Pt-rich cases. However, for completeness, we show some results for the Au-rich alloys as well.

III. RESULTS

A. Grain boundary energy

Before discussing the segregation behavior, we calculate the energies of the three GBs using the VASP method. The results are collected in Fig. 3. For pure Pt, the calculated GB energies for the Σ3(111), Σ5(310), and Σ9(221) GBs are 0.146, 0.910, and 0.787 J/m^2, respectively. For pure Au, these energies are 0.004, 0.415, and 0.347 J/m^2, respectively. In general, the present GB energies have a good agreement with the former DFT values.[37,39,40] The slight discrepancies may be due to the different calculation parameters, such as potential, *k*-mesh, structural relaxation, and exchange-correlation approximation.

Here, we should make two observations. First, the GB energies of Au are substantially smaller, in general, than the GB energies of Pt. Second, the close-packed GB always has the smallest formation energy and this energy is much smaller than the formation energies of the more open GBs. The smaller GB formation energies of Au compared to Pt suggest that at low temperatures, where the configurational entropy can be neglected, the pure GB effects always favor Au near the interface in both Pt-rich and Au-rich alloys. However, the segregation energy is controlled by both bulk and GB effects, especially in the case of concentrated alloys and, therefore, a full segregation study is required before making a solid conclusion.

B. Segregation energy

For the EMTO segregation studies, we used the relaxed GB structures obtained in the VASP calculations. For Pt-rich alloys, we used the structures obtained for pure Pt and, for Au-rich alloys, the structures obtained for pure Au. To investigate the segregation behavior in alloys at static conditions, a matrix atom near the GB was substituted by a solute atom. Four symmetrically different sites were selected for this study as shown in Fig. 1.

The VASP and EMTO segregation energies for the dilute alloys are plotted in Fig. 4. Here, we consider only the dilute systems, meaning that the solute concentration is zero at all sites except the selected GB sites. By definition, a negative segregation energy indicates that the solute atom tends to stay at the GB position, while a positive segregation energy indicates that the solute atom tends to stay in the grain interior. As shown in Fig. 4, on the Pt-rich side, the segregation energy of Au at site s2 (for notations, see Fig. 1) of these three GBs is the lowest compared to the other sites, implying that s2 is the most favorable site for Au segregation. On the other hand, it is found that the segregation energy for the close-packed Σ3(111) GB is small, being −0.012 eV, which means that the segregation of Au at the Σ3(111) GB is weak. For the Σ5(310) and Σ9(221) GBs, the segregation energies are −0.734 and −0.537 eV, respectively, which means that there is a strong tendency for Au to segregate toward these two open GBs. On the Au-rich side of the phase diagram, the segregation energies of Pt at

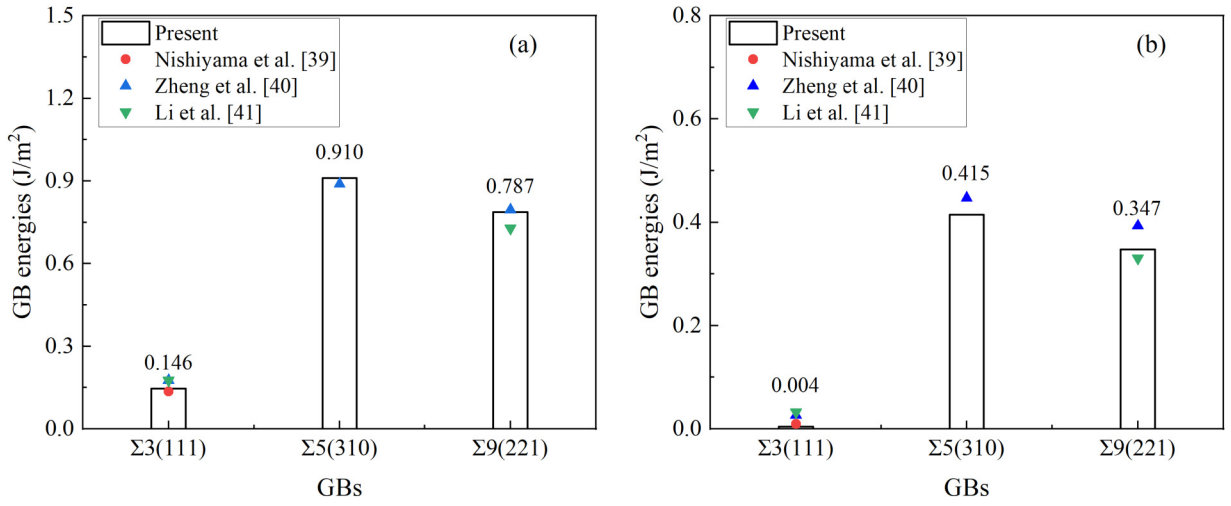

FIG. 3. GB energies for Pt (a) and Au (b) calculated using the VASP method. The former DFT values[37,39,40] are listed for comparison.

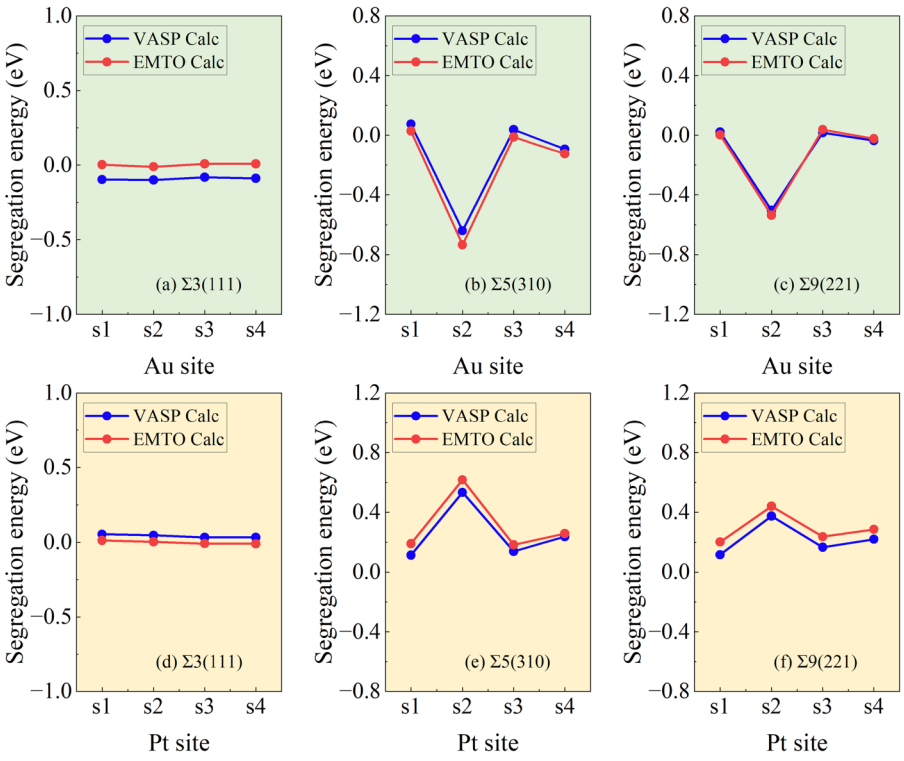

FIG. 4. GB segregation energies of the solute atom at different sites: (a)–(c) for the Pt-rich alloys; (d)–(f) for the Au-rich alloys. See Fig. 1 for notations of the s1, s2, s3, and s4 GB sites.

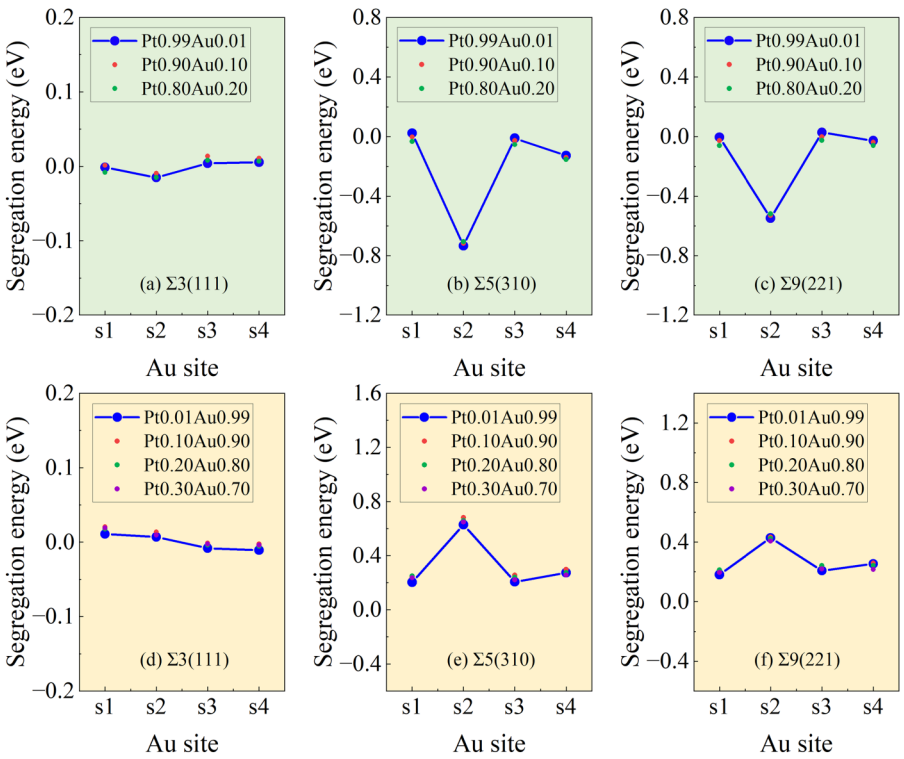

FIG. 5. The bulk composition dependence of the segregation energy: (a)–(c) for the Pt-rich alloys; (d)–(f) for the Au-rich alloys. All calculations were done using the EMTO method.

different sites are all positive, indicating that Pt has a strong anti-segregation tendency. That is, Pt prefers to reside in the Au grain interior rather than at the GBs in Au-rich alloys.

Comparing the two sets of data in Fig. 4, we find that the EMTO results deviate slightly from the VASP results; however, the trends are consistent. This confirms that the segregation behavior of solutes can be consistently evaluated with these two methods. This finding is especially important, since with the EMTO method, we can now go further and study the concentrated alloys as well. In addition, according to Fig. 4, both EMTO and VASP results show that Au tends to segregate at Pt GBs, while Pt cannot segregate at Au GBs. This prediction is consistent with the experimental results[10,14] and other theoretical calculations.[17,19]

Figure 5 shows the effect of bulk composition on the segregation energy calculated using the EMTO method. It is noticed that the trends in the segregation energies for concentrated alloys are similar to those of the dilute systems, and the change in the segregation energy is small for both the Pt-rich side and Au-rich side of the phase diagram. We also plotted the segregation energy from Pt-rich to Pt-poor systems (see Fig. S4 in the supplementary material). It can be seen that the segregation energy of the Σ3(111) GB fluctuates around zero over the range of Pt–Au compositions, suggesting that solute segregation at the Σ3(111) GB is energetically unfavorable. For the two open GBs, the segregation energy transitions from negative to positive with increasing Au concentration, and this transition is particularly pronounced for the s2 site. The transition of segregation energy can be attributed to the "site saturation effect," where segregation occurs first at the most favorable GB sites, and once these sites are occupied, more solute atoms must segregate to less favorable sites. This results in a reduced tendency to segregate with increasing solute concentration.[24] In addition, as the system transitions toward a Pt-poor composition (e.g., $Pt_{0.01}Au_{0.99}$), Au atoms become the dominant species, and the Au–Au interactions become increasingly significant. In this case, the strong Au–Au interaction favors the homogeneous distribution of Au atoms in the bulk, while the segregation of Au at the GB site may induce large local lattice distortion, making the segregation at GB thermodynamically unfavorable. This leads to an anti-segregation behavior of Au, which is particularly pronounced at the GB s2 site due to the volume effect.

In these calculations, the GB structures were fixed to those optimized by VASP for pure metals. Additional structural changes induced by bulk chemistry could alter the results from Fig. 5. In order to verify this effect, we carried out segregation studies using the GB structures obtained for the other side of the phase diagram. Namely, we used for Au-rich alloys the structures obtained for Pt, and vice versa. The results (not shown) are practically the same as those shown in Fig. 5. Therefore, we conclude that the bulk composition and the precise local structure around the GB have a minor influence on the segregation energy in $Pt_{1-c}Au_c$ alloys.

C. The effect of temperature

Since the segregation energies for Pt are all positive for the Au-rich alloys, in the following, we consider the temperature effect on the GB segregation for the Pt-rich alloys only. This choice is also motivated by the initial goal to study the temperature-induced segregation behavior in Pt-rich alloys. Nevertheless, since the absolute values of the segregation energies for the two alloy families are similar, we expect that conclusions obtained for the Pt-rich alloys remain the same for the Au-rich alloys, but with opposite signs.

The segregation energy calculations show that for Pt-rich alloys, site s2 exhibits strong segregation while the other sites display weak or anti-segregation. Therefore, the two sites s1 and s2 are chosen to analyze the segregation behavior at the selected GBs. We should notice that considering all GB sites in the segregation study is, in principle, possible; however, that would substantially increase the computation time being a multi-dimensional problem compared to a two-dimensional problem. In other words, we limit ourselves to $N = 2$ in Eq. (5). We select these two sites for segregation study also because they show very different behaviors and, therefore, can be considered as representative for two typical GB sites.

The GB segregation profiles for the three GBs have been determined for $c = 0.01$, 0.10, and 0.20 bulk compositions and for $T = 10$, 300, 600, 900, and 1200 K. The segregation profile is described in terms of the equilibrium c_1 and c_2 GB concentrations at sites s1 and s2, respectively. The equilibrium concentrations, in turn, are obtained by minimizing the Gibbs energy in Eq. (5) at each temperature against c_1 and c_2. To obtain a more accurate and robust estimate of the equilibrium concentration, a polynomial fit was used to find the Gibbs energy minimum. Details of polynomial fitting are given (Fig. S7 in the supplementary material).

The bar graphs in Fig. 6 show the segregation profiles of the three GBs obtained by polynomial fitting at different temperatures. For the Σ3(111) GB [Fig. 6(a)], the Au segregation at sites s1 and s2 is found to be energetically favorable at low temperatures. At dilute bulk alloy ($c = 0.01$), c_1 and c_2 decrease very quickly with temperature. When the temperature reaches 300 K, c_1 and c_2 drop close to zero. At 10% Au in the bulk, the GB Au concentrations decrease slower with increasing temperature compared to the dilute alloy case. Nevertheless, around 600 K, both c_1 and c_2 drop nearly to the bulk concentration level, and the system becomes homogeneous. At 20% Au in the bulk, the concentration profile approaches the bulk value at the highest temperature considered (1200 K), with a small deviation attributable to the polynomial fitting used to determine the equilibrium concentration. In other words, when about 20% Au is added to Pt, the close-packed GB becomes homogeneous only around 1200 K.

For the Σ5(310) GB [Fig. 6(b)], the Au segregation at site s1 is strongly temperature-dependent for all three bulk concentrations. In particular, for dilute bulk alloy ($c = 0.01$), c_1 drops from 100% to zero as the temperature increases from zero to 600 K. However, for $c = 0.10$, 0.20, c_1 remains far above the bulk value even at 1200 K. For instance, in 20% Au alloy, the concentration at site s1 at 1200 K is more than twice the bulk value. The segregation at site s2 is even more pronounced. At low bulk concentration ($c = 0.01$), the Au concentration at site s2 drops to 86% at 1200 K, but at high bulk concentrations ($c = 0.10$, 0.20), even the highest temperatures considered here are not enough to block full Au segregation. This situation is completely different from the one predicted for the Σ3(111) GB.

The segregation profile for the Σ9(221) GB [Fig. 6(c)] is similar to, but slightly weaker than that of the Σ5(310) GB. The Au segregation at site s1 is temperature-dependent. For site s2, c_2

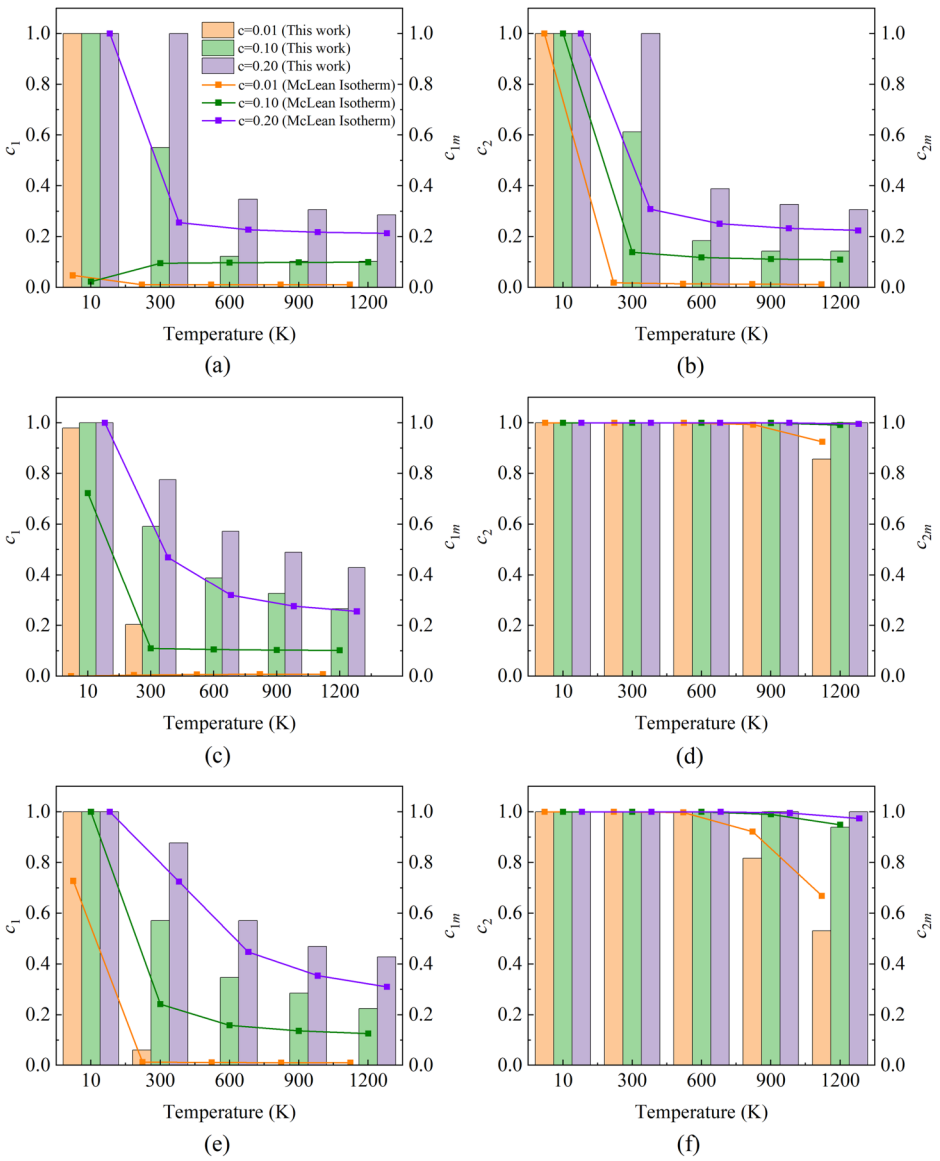

FIG. 6. GB segregation profiles for the Pt-rich alloys at different temperatures. c_1 and c_2 represent the Au concentration for site s1 and s2, respectively. Zero segregation concentration is not shown in the figure. The bar graphs show the segregation profiles obtained by polynomial fitting, while the solid lines and the subscript m correspond to the results calculated by the McLean isotherm. Results are shown for (a) and (b) Σ3(111) GB, (c) and (d) Σ5 (310) GB, and (e) and (f) Σ9(221) GB.

remains constant below 900 K, regardless of the bulk compositions. At high temperatures, the Au segregation at site s2 is weakly bulk composition-dependent. At $c = 0.01$, c_2 decreases to 82% at 900 K, and at $c = 0.10$, c_2 decreases to 94% at 1200 K. When the Au concentration in the bulk is 20%, a temperature higher than 1200 K is needed to move Au from site s2 into the bulk.

The above results show that there is a very strong segregation at both open GBs. It is predicted that for open GBs, extremely high temperatures are required to eliminate Au segregation and achieve homogeneity. To date, theoretical analysis of Au segregation is scarce. Udler and Seidman[19] studied the equilibrium segregation at the Σ5(310) tilt GB for a Pt–1 at. % Au alloy with Monte Carlo simulations. The segregation profile at 850 K shows that site s2 is rich in Au, while site s1 has only a small amount of Au segregation. Although quantitative comparisons cannot be made, their segregation profiles for Pt–1 at. % Au alloy at the Σ5(310) GB is in reasonable agreement with our results.

The McLean isotherm is a classic approach to model the enrichment at elevated temperatures for dilute systems. To further illustrate the advantage of our method for accurate modeling of the segregation concentrations in the concentrated alloy systems, we made a comparison between the results calculated by Eq. (5) and those obtained using the McLean isotherm. The McLean treatment employs the equation described in Ref. 24. The solid line in Fig. 6 shows the GB segregation profiles based on the Mclean isotherm. For the Σ3(111) GB, the segregation concentrations c_1 and c_2

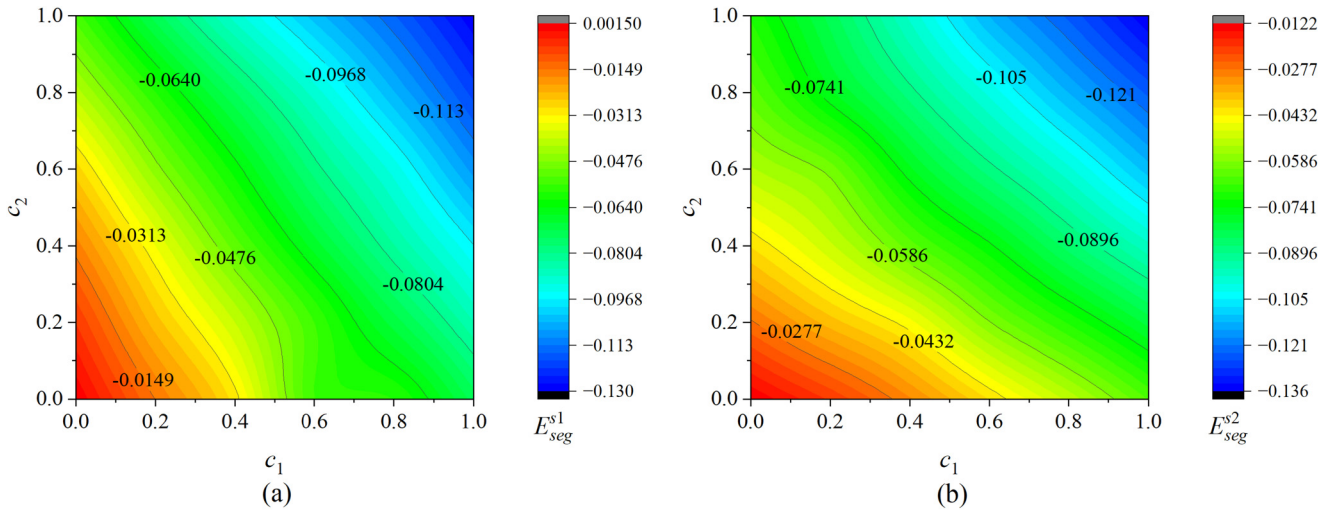

FIG. 7. Segregation energy for site s1 (a) and site s2 (b) of the Σ3(111) GB. Unit is eV. See the text for notations.

calculated for the dilute system ($c = 0.01$) by the two methods are similar except for $T = 10$ K. Specifically, Eq. (5) predicts a very high c_1 whereas the Mclean isotherm predicts a c_1 close to zero at 10 K. This is because in Eq. (5), whenever there is a segregation site with the lowest relative energy, then the system will tend to segregate to that site even if the segregation energy is very small or positive. Conversely, the McLean isotherm predicts weak or no segregation under similar conditions (small or positive segregation energy). This prediction is supported by the olive-colored line in Fig. 6(a) for a bulk composition of $c = 0.10$, which shows minimal Au segregation at 10 K due to the positive segregation energy. However, as the temperature increases, c_1 gradually increases until it approaches the bulk concentration. In addition, for the concentrated alloy system ($c = 0.10$, 0.20), the values of c_1 and c_2 derived from Eq. (5) are higher than those derived from the McLean isotherm in the range of 300–120 K. This could be because the McLean isotherm ignores the increasing solute–solute interaction beyond the dilute limit.[24] The strong solute–solute interactions promote the segregation at GB and, thus, increases the segregation concentration. For the two open GBs, the segregation trend for the less attractive site s1 is similar to that of the Σ3(111) GB, i.e., the McLean treatment may underestimate the segregation concentration of the less attractive site for the concentrated alloy system. However, it is interesting to note that for site s2 with strong segregation tendency, for both dilute and concentrated alloy systems, the segregation concentration c_2 derived from the McLean isotherm agrees well with that derived from Eq. (5), especially at medium temperature (300–600 K). At a high temperature, Eq. (5) predicts a higher segregation concentration than the McLean isotherm, except for the dilute system. Thus, it can be inferred that the strong segregation energy dominates at low temperatures, leading to similar results for both approaches. However, at high temperatures, configurational entropy plays a more significant role in the concentrated alloys. Equation (5) captures this effect better, hence predicting a higher segregation concentration. The above findings, thus, demonstrate the importance of our method for the accurate treatment of concentrated alloy systems at finite temperature.

IV. DISCUSSION

A. Chemical driving force of Au segregation in Pt-rich alloys

The present results suggest that the Au distribution in Pt-rich alloys is highly anisotropic and heterogeneous. The concentration profile depends on the GB character, temperature, and bulk composition. To shed light on the solute segregation behavior at different GB sites, in the following, we further analyze the segregation energy as functions of c_1 and c_2 at 0 K and bulk composition $c = 0$. All discussions in this section refer to such dilute Pt–Au alloys.

Figure 7 displays the segregation energy for sites s1 and s2 of the Σ3(111) GB. The two contour maps in Fig. 7 show very similar patterns. The segregation energy for site s1 decreases as c_1 and c_2 increase and ranges from 0.0015 to −0.130 eV. The trend in Fig. 7(a) indicates that the Au segregation at site s1 is nearly zero or weak, but the segregation degree increases as the GB concentration increases. Similarly, the segregation energy for site s2 decreases with increasing c_1 and c_2, but its value is slightly more negative than that for site s1. This means that the Au segregation at site s2 is weak but slightly stronger than at site s1. It is interesting to observe that for both s1 and s2 sites, the segregation tendency increases with increasing c_1 and c_2, which means that the more Au we have in either site s1 or s2, the larger the segregation driving force becomes.

Figure 8 displays the segregation energy for sites s1 and s2 of the Σ5(310) GB. The segregation energy for site s1 [Fig. 8(a)] is small (close to zero), which suggests that the segregation of Au at site s1 is negligible. In contrast, the segregation energy for site s2 [Fig. 8(b)] is large and negative, ranging from −0.672 to −0.852 eV.

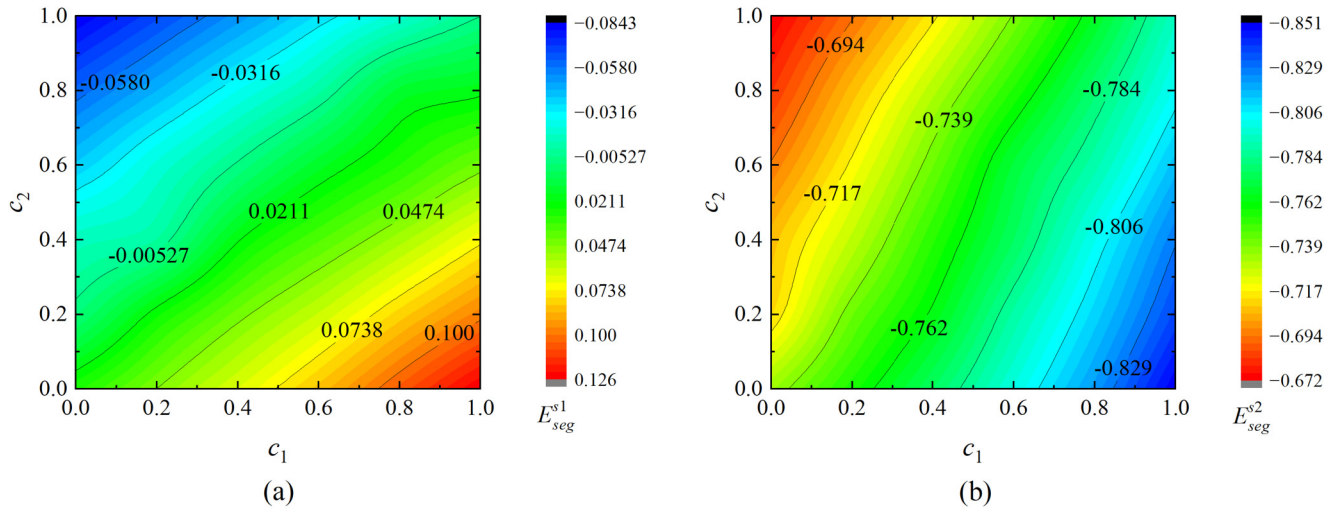

FIG. 8. Segregation energy for site s1 (a) and site s2 (b) of the Σ5(310) GB. Unit is eV. See the text for notations.

This means that the Au segregation at site s2 is very strong irrespective of the concentrations c_1 and c_2.

We should observe that the segregation tendency for site s1 is increased (decreased) by increasing c_2 (c_1), whereas the segregation tendency for site s2 is increased (decreased) by increasing c_1 (c_2). This behavior is opposite to the one observed for the close-packed GB. In particular, for the Σ3(111) GB, the concentrations for the s1 and s2 sites have similar effects on the driving force for segregation: increasing c_1 or c_2 makes the segregation energy more negative. However, for the Σ5(310) GB, increasing the concentration of site s2 induces segregation for s1 but diminishes the segregation for s2. On the other hand, increasing the concentration of site s1 lowers the segregation for s1 but enhances the segregation for s2. We conclude that increasing the Au level on a particular GB site always decreases the tendency for further Au segregation to that particular site. However, there is a chemical interaction between the two GB sites which manifests in mutually induced segregation tendencies.

The trends for the segregation energy of the Σ9(221) GB (Fig. 9) are in between those of the Σ3(111) and Σ5(310) GBs. In particular, the pattern for the segregation energy for site s1 of the Σ9(221) GB resembles that of site s1 of Σ5(310), whereas the pattern for the segregation energy for site s2 of the Σ9(221) GB resembles that of site s2 of Σ3(111). The segregation energy for site s1 [Fig. 9(a)] is close to zero, implying that the segregation of Au at

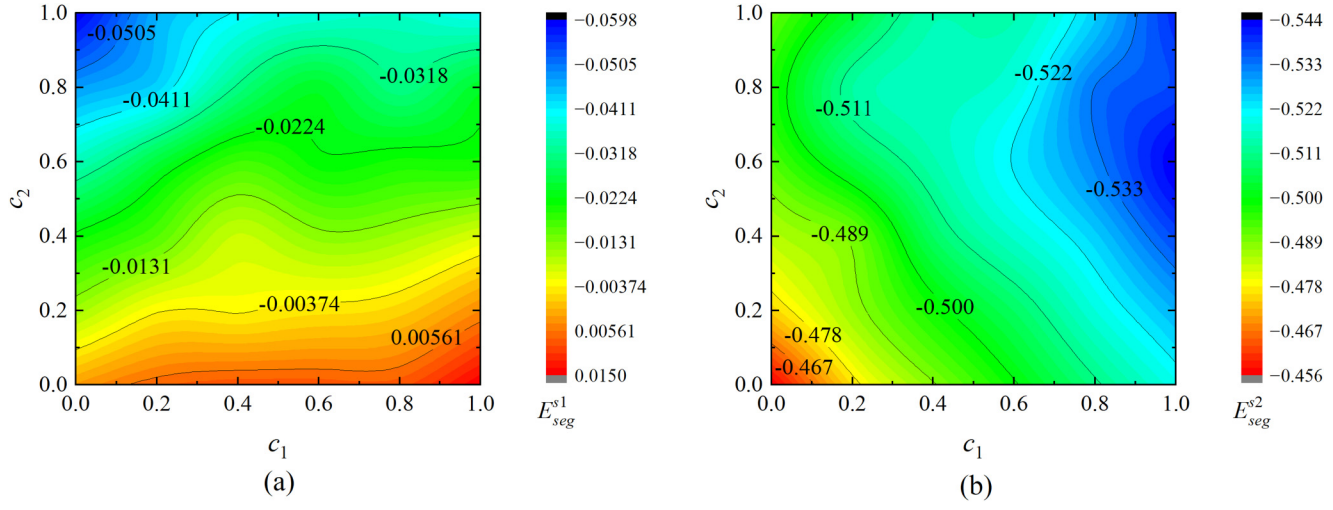

FIG. 9. Segregation energy for site s1 (a) and site s2 (b) of the Σ9(221) GB. Unit is eV. See the text for notations.

site s1 is weak. The segregation energy for site s2 [Fig. 9(b)] is negative with values ranging from −0.456 to −0.544 eV, meaning that the Au segregation at site s2 is strong.

The above segregation energy analyses show that for the close-packed GB, there is a weak chemical driving force for Au segregation to the GB and this driving force increases with Au concentration at the GB. However, for the open GBs, not all GB sites attract Au in dilute Pt-rich alloys. For these GBs, site s1 has a small positive segregation energy, whereas site s2 has a large negative segregation energy making it very attractive to Au. For all GBs, there is a marked interaction between the GB sites. In particular, the segregation to site s2 induces segregation to site s1 and vice versa.

B. Volume effect of Au segregation in Pt-rich alloys

For a possible explanation of the pronounced Au segregation, especially to site s2, we collected the atomic volumes of the GB sites ($V_a^{s_i}$) and the bulk site (V_a^b) in Table II. The numbers in the table refer to Pt-based dilute alloys, and, thus, we have $V_a^b = V_a^{\mathrm{Pt}} = 15.848$ Å^3. Since the atomic volume of Au ($V_a^{\mathrm{Au}} = 18.180$ Å^3) is ∼15% larger than that of Pt, it prefers sites with large local (Voronoi) volume. For the close-packed GB, the atomic volume of site s2 is only slightly larger than the bulk value, whereas site s1 has the nearly the same volume as in the bulk. We notice that the differences are very small, and they can slightly change depending on the details of the structural relaxation and numerical details. Therefore, based on volume arguments, we conclude that Au should not segregate to the close-packed GB. The weak segregation discussed in Secs. III B and III C should, therefore, be driven mostly by chemical effects.

For both open GBs, we have $V_a^{s_2} \gg V_a^{s_1} > V_a^b$. In particular, the atomic volume of site s2 is very different from the bulk value and $V_a^{s_2} \gtrsim V_a^{\mathrm{Au}}$ for both open GBs. On the other hand, the atomic volume of site s1 is relatively small, namely, $V_a^{s_1} < V_a^{\mathrm{Au}}$, and the difference between $V_a^{s_1}$ and V_a^{Pt} is only 2%–4%. The very large local volume near site s2 makes this position favorable for Au. This is reflected by the large negative segregation energy in Figs. 8 and 9 already for $c_1 = c_2 = 0$. The situation is similar to the free surfaces of Pt, where Au is known to segregate.[47] The above findings indicate that the initial Au segregation to the open GBs is strongly influenced by the local environment, especially by the local atomic volume near the GB sites. The above arguments are expected to apply to all open GBs, which have at least one site with the local atomic volume similar to or larger than that of pure Au.

The coupling between the segregation behavior of sites s1 and s2 can be explained as follows. Initially, only s2 has a large driving force for Au segregation due to the large local volume around this site. As soon as Au builds up at s2, the local Au concentration near the GB increases. In bulk Pt–Au alloys, at low temperatures, there is a strong tendency for phase separation [see Fig. 2(a)]. In particular, the homogeneous Pt–Au system separates into Pt- and Au-rich alloys. Actually, temperatures around 900 K are needed to form Pt-rich solid solutions with few percent of Au content. Assuming a similar phase diagram near the GB, the increased Au concentration near site s2 acts as a nucleation site for phase separation and brings more Au to the nearest sites, such as s1. We argue that this interaction is the reason for the aforementioned strong coupling between the concentration of site s2 and the driving force for segregation for site s1. This effect is clearly visible in Figs. 7–9, where increasing c_2 always makes the segregation energy for site s1 more negative, i.e., enhances the originally small or even missing driving force for Au segregation at site s1.

TABLE II. Voronoi atomic volume (in units of Å^3) for the GB (s1 and s2) and bulk sites for the three GBs.

Site	Σ3(111)	Σ5(310)	Σ9(221)
s1	15.848	16.226	16.410
s2	15.850	19.703	18.193
Bulk	15.848	15.848	15.848

In addition to comparing the atomic volumes, we can also calculate the elastic energy contribution due to lattice mismatches between matrix and solute atoms to analyze the segregation for different GBs.[48,49] According to the equation described in the literature,[48] we calculated the elastic energy contribution ΔE_{Au}^V, which represent the volume elastic effects caused by the segregation of Au at Pt GBs. The calculation details are given in the supplementary material. The positive volume elastic effect represents an increase in elastic energy near the GB, so this segregant is not energetically favored. ΔE_{Au}^V in the Σ3(111), Σ5(310), and Σ9(221) GBs are 0.02, −0.30, and −0.41 eV, respectively, which means that Au at open GBs introduces a beneficial volume effect due to its larger atomic size. In other words, the volume elastic effect promotes the segregation of Au at Pt GBs, except for the close-packed GB.

C. Electron localization function

To further understand the mechanism of segregation in GBs at the atomic level, the electron localization function is calculated. As shown in Fig. 10, for the close-packed GB, when Au occupies sites s1 and s2, the charge density is similar to that of the bulk, indicating that the close-packed GB does not attract Au and has no strong preference for sites s1 and s2. For the two open GBs, when Au occupies site s2, the charge density of the GB region is increased compared to the bulk region, which enhances GB bonding and makes the system more energetically stable. Conversely, when Au occupies site s1, the charge density of the GB region is decreased, which weakens the GB bonding. This also explains why Au prefers site s2 over site s1.

D. Segregation anisotropy

Previous experiments and atomic simulations show that at 773 and 973 K, Au displays no segregation at close-packed GBs, but open GBs are enriched in Au.[10,14] On the other hand, the present results show that the segregation of Au is energetically favorable at both close-packed and open GBs for temperatures below ∼600 K. However, a tendency for segregation at such temperature conditions does not necessarily mean that a concentration profile can, indeed, be observed under realistic conditions. This is because segregation strongly depends on the diffusivity of the solute in bulk and GB regions. According to the Arrhenius relations for Au in Pt,[50] the diffusion coefficient of Au in Pt is around 1.55×10^{-23} cm^2/s at 600 K

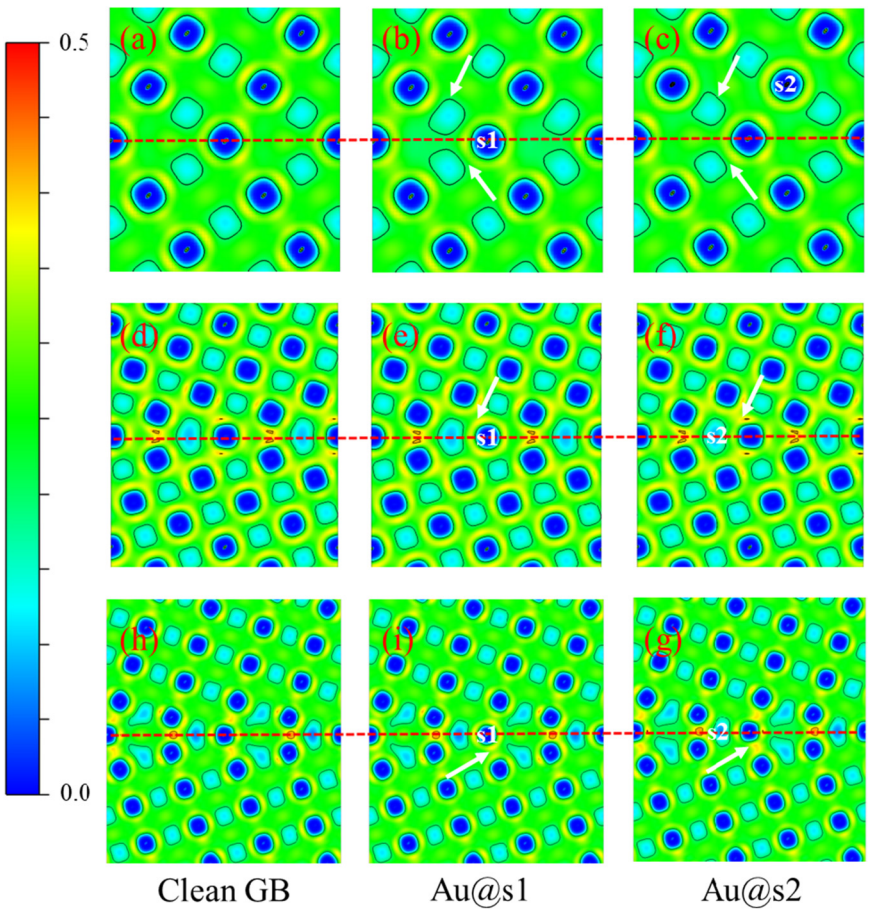

FIG. 10. Electron localization function for three GBs on the plane x = 1: (a)–(c) for Σ3 (111) GB, (d)–(f) for Σ5 (310) GB, and (h)–(g) for Σ9 (221) GB. The white arrow points to regions having different charge densities. The charge density diagram is expanded twice for clearer viewing.

and 1.15×10^{-16} at 900 K. Thus, although Au enrichment is energetically favored in both close-packed and open GBs below 600 K, it would take a long time for Au to diffuse to these GBs. This situation is similar to the formation of $L1_0$–FeNi.[51] The order–disorder transition temperature of $L1_0$–FeNi is around 600 K. Due to the small diffusion coefficient of Ni in Fe ($\sim 1.2 \times 10^{-25}$ cm^2/s at 600 K),[52] it requires a very long time to form this compound; so, $L1_0$–FeNi can only be found naturally in meteorites.

As the temperature increases to a point where diffusion is expected to be effective, such as 900 K, Au segregation to the open GBs is distinct. However, due to the weak chemical driving force for the close-packed GB, the configurational entropy overcomes the chemical effect at high temperatures, resulting in no Au segregation to the close-packed GB.

V. CONCLUSIONS

In the present work, we studied the impact of bulk composition and temperature on the segregation behaviors of three symmetric tilt GBs in $Pt_{1-c}Au_c$ alloys. The theoretical predictions were derived from *ab initio* calculations carried out within the density functional theory framework as implemented in VASP and EMTO software. The thermal properties were determined from the temperature-dependent Gibbs energy, which was assessed in the case of the bulk phase diagram of Pt–Au. The main results are

(1) The GB energies and the segregation energies for the three types of GBs were calculated at 0 K using VASP and EMTO. The results show that on the Pt-rich side, Au tends to segregate for all three GBs, and the segregation is not sensitive to the bulk composition. On the Au-rich side, Pt tends to stay in the bulk rather than at the GBs.
(2) The physical mechanism for Au segregation in Pt-rich alloys is the large local atomic volume near the open GB sites combined with the wide miscibility gap in Pt–Au alloys. For the close-packed GB, the driving force for Au segregation is much weaker compared with that of the open GBs.
(3) When the configurational entropy is considered at finite temperatures, the Au segregation profiles show that the close-packed Σ3(111) GB is energetically favorable for Au enrichment at low temperatures. However, due to the negligible diffusion coefficient at such temperatures, it is difficult to observe Au segregation at the Σ3(111) GB.

(4) For the two open GBs, Σ5(310) and Σ9(221), due to their much larger chemical driving force than that of the close-packed GB, the configurational entropy is insufficient to affect the segregation behaviors. Therefore, Au is rich in the open GBs at high temperatures.

Based on these, the segregation anisotropy in Pt–Au alloys can be explained by a competition between the chemical driving force and the configurational entropy. The main conclusions also contribute to understanding the GB segregation anisotropy in similar alloy systems. Furthermore, the methodology employed in this work can be generalized to other binary or multi-component dilute or concentrated alloys while the composition variation should be considered.

SUPPLEMENTARY MATERIAL

See the supplementary material for the convergence test, ECP calculations, Gibbs energy polynomial fit, and volume elastic effect calculations.

ACKNOWLEDGMENTS

This work was supported by the National Natural Science Foundation of China (NNSFC) (No. 12172038), the Scientific and Technological Project of Yunnan Precious Metals Laboratory (YPML-20240502034), and the China Scholarship Council. The calculations were performed on resources provided by the National Academic Infrastructure for Supercomputing in Sweden (NAISS) at the National Supercomputer Centre (NSC) in Linköping through Grant Agreement No. 2024-5-10. X.Y. acknowledges Song Lu and Ziyi Xiong for their guidance. L.V., C.L., and W.L. acknowledge the Swedish Research Council, Swedish Foundation for Strategic Research, the Hungarian Scientific Research Fund (OTKA Grant No. 128229), the Carl Tryggers Foundation (Grant Nos. 19:325 and 20:474), and the Formas—a Swedish Research Council for Sustainable Development (Grant No. 2023-00543).

AUTHOR DECLARATIONS

Conflict of Interest

The authors have no conflicts to disclose.

Author Contributions

Xin Yao: Investigation (equal); Methodology (equal); Software (equal); Validation (equal); Visualization (equal); Writing – original draft (equal). **Ya-Fang Guo:** Conceptualization (equal); Funding acquisition (equal); Project administration (equal); Resources (equal); Supervision (equal); Writing – review & editing (equal). **Wei Li:** Methodology (equal); Resources (equal); Software (equal); Writing – review & editing (equal). **Kalevi Kokko:** Methodology (equal); Validation (equal); Writing – review & editing (equal). **Changle Li:** Validation (equal); Writing – review & editing (equal). **Levente Vitos:** Funding acquisition (equal); Methodology (equal); Project administration (equal); Resources (equal); Software (equal); Supervision (equal); Writing – review & editing (equal).

DATA AVAILABILITY

The data that support the findings of this study are available from the corresponding authors upon reasonable request.

REFERENCES

[1]J. F. Curry, T. F. Babuska, T. A. Furnish, P. Lu, D. P. Adams, A. B. Kustas, B. L. Nation, M. T. Dugger, M. Chandross, B. G. Clark, B. L. Boyce, C. A. Schuh, and N. Argibay, "Achieving ultralow wear with stable nanocrystalline metals," Adv. Mater. **30**, 1802026 (2018).
[2]R. Völkl, D. Freund, A. Behrends, B. Fischer, J. Merker, and D. Lupton, "Platinum base alloys for high temperature space applications," Mater. Transp. Technol. **1**, 257–260 (2000).
[3]G. Rakhtsaum, "Platinum alloys: A selective review of the available literature," Platin. Met. Rev. **57**, 202–213 (2013).
[4]W. Yu, X. Chong, M. Gan, Y. Wei, A. Zhang, Y. Wang, and J. Feng, "Exploring the solution strengthening effect of 33 alloying elements in Pt-based alloys by high-throughput first-principles calculations," J. Appl. Phys. **131**, 185103 (2022).
[5]J. Hu, M. Xie, Y. Chen, J. Fang, and Q. Zhang, "Thermodynamic reassessment of Au-Pt-Sn system," Mater. Res. Express **9**, 016507 (2022).
[6]V. Papaefthimiou, M. Diebold, C. Ulhaq-Bouillet, W. H. Doh, R. Blume, S. Zafeiratos, and E. R. Savinova, "Potential-induced segregation phenomena in bimetallic PtAu nanoparticles: An *in situ* near-ambient-pressure photoelectron spectroscopy study," ChemElectroChem **2**, 1519–1526 (2015).
[7]W. Tang, S. Jayaraman, T. F. Jaramillo, G. D. Stucky, and E. W. Mcfarland, "Electrocatalytic activity of gold–platinum clusters for low temperature fuel cell applications," J. Phys. Chem. C **113**, 5014–5024 (2009).
[8]X. Zhou, O. Kasian, T. Luo, S.-H. Kim, C. Zhang, S. Zhang, S. Lee, G. B. Thompson, G. Dehm, B. Gault, and D. Raabe, "Chemical partitioning at crystalline defects in PtAu as a path way to stabilize electrocatalysts," ArXiv:2209.13166 (2022), pp. 1–24.
[9]A. S. Darling, "Gold-platinum alloys," Platin. Met. Rev. **6**, 106–111 (1962).
[10]P. Lu, F. Abdeljawad, M. Rodriguez, M. Chandross, D. P. Adams, B. L. Boyce, B. G. Clark, and N. Argibay, "On the thermal stability and grain boundary segregation in nanocrystalline PtAu alloys," Materialia **6**, 100298 (2019).
[11]G. C. Bond, "The electronic structure of platinum-gold alloy particles," Platin. Met. Rev. **51**, 63–68 (2007).
[12]D. Raabe, M. Herbig, S. Sandlöbes, Y. Li, D. Tytko, M. Kuzmina, D. Ponge, and P. P. Choi, "Grain boundary segregation engineering in metallic alloys: A pathway to the design of interfaces," Curr. Opin. Solid State Mater. Sci. **18**, 253–261 (2014).
[13]P. Lejček, M. Šob, and V. Paidar, "Interfacial segregation and grain boundary embrittlement: An overview and critical assessment of experimental data and calculated results," Prog. Mater. Sci. **87**, 83–139 (2017).
[14]C. M. Barr, S. M. Foiles, M. Alkayyali, Y. Mahmood, P. M. Price, D. P. Adams, B. L. Boyce, F. Abdeljawad, and K. Hattar, "The role of grain boundary character in solute segregation and thermal stability of nanocrystalline Pt-Au," Nanoscale **13**, 3552–3563 (2021).
[15]A. Seki, D. N. Seidman, Y. Oh, and S. M. Foiles, "Monte Carlo simulations of segregation at [001] twist boundaries in a Pt(Au) alloy—I. Results," Acta Metall. Mater. **39**, 3167–3177 (1991).
[16]A. Seki, D. N. Seidman, Y. Oh, and S. M. Foiles, "Monte Carlo simulations of segregation at [001] twist boundaries in a Pt (Au) alloy—II. Discussion," Acta Metall. Mater. **39**, 3179–3185 (1991).
[17]D. Udler and D. N. Seidman, "Solute-atom segregation at high-angle (002) twist boundaries in dilute Au-Pt alloys," J. Mater. Res. **10**, 1933–1941 (1995).
[18]J. D. Rittner, D. Udler, D. N. Seidman, and Y. Oh, "Atomic scale structural effects on solute-atom segregation at grain boundaries," Phys. Rev. Lett. **74**, 1115–1118 (1995).
[19]D. Udler and D. N. Seidman, "Solute segregation at [001] tilt boundaries in dilute fcc alloys," Acta Mater. **46**, 1221–1233 (1998).

[20]J. L. Priedeman and G. B. Thompson, "The influence of alloying in stabilizing a faceted grain boundary structure," Acta Mater. **201**, 329–340 (2020).
[21]C. J. O'Brien, C. M. Barr, P. M. Price, K. Hattar, and S. M. Foiles, "Grain boundary phase transformations in PtAu and relevance to thermal stabilization of bulk nanocrystalline metals," J. Mater. Sci. **53**, 2911–2927 (2018).
[22]C. Baruffi and W. A. Curtin, "Theory of spontaneous grain boundary roughening in high entropy alloys," Acta Mater. **234**, 118011 (2022).
[23]D. Scheiber, V. I. Razumovskiy, P. Puschnig, R. Pippan, and L. Romaner, "*Ab initio* description of segregation and cohesion of grain boundaries in W-25 at. % Re alloys," Acta Mater. **88**, 180–189 (2015).
[24]M. Wagih and C. A. Schuh, "Grain boundary segregation beyond the dilute limit: Separating the two contributions of site spectrality and solute interactions," Acta Mater. **199**, 63–72 (2020).
[25]J. Y. Yan, H. Ehteshami, P. A. Korzhavyi, and A. Borgenstam, "Σ3(111) grain boundary of body-centered cubic Ti–Mo and Ti–V alloys: First-principles and model calculations," Phys. Rev. Mater. **1**, 023602 (2017).
[26]L. Huber, B. Grabowski, M. Militzer, J. Neugebauer, and J. Rottler, "*Ab initio* modelling of solute segregation energies to a general grain boundary," Acta Mater. **132**, 138–148 (2017).
[27]T. Tsuru, H. Somekawa, and D. C. Chrzan, "Interfacial segregation and fracture in Mg-based binary alloys: Experimental and first-principles perspective," Acta Mater. **151**, 78–86 (2018).
[28]D. Scheiber, M. N. Popov, and L. Romaner, "Temperature dependence of solute segregation energies at W GBs from first principles," Scr. Mater. **222**, 115059 (2023).
[29]M. Ropo, K. Kokko, L. Vitos, J. Kollár, and B. Johansson, "The chemical potential in surface segregation calculations: AgPd alloys," Surf. Sci. **600**, 904–913 (2006).
[30]L. Vitos, "Total-energy method based on the exact muffin-tin orbitals theory," Phys. Rev. B **64**, 1–11 (2001).
[31]L. Vitos, H. L. Skriver, B. Johansson, and J. Kollár, "Application of the exact muffin-tin orbitals theory: The spherical cell approximation," Comput. Mater. Sci. **18**, 24–38 (2000).
[32]J. P. Perdew, K. Burke, and M. Ernzerhof, "Generalized gradient approximation made simple," Phys. Rev. Lett. **77**, 3865–3868 (1996).
[33]P. Soven, "Coherent-potential model of substitutional disordered alloys," Phys. Rev. **156**, 809–813 (1967).
[34]R. Substitutional Alloys and B. L. Gyorffy, "Coherent-potential approximation for a nonoverlapping-muffin-tin-potential model of random substitutional alloys," Phys. Rev. B **5**, 2382–2384 (1972).
[35]G. Kresse and J. Furthmüller, "Efficiency of ab-initio total energy calculations for metals and semiconductors using a plane-wave basis set," Comput. Mater. Sci. **6**, 15–50 (1996).
[36]P. E. Blöchl, "Projector augmented-wave method," Phys. Rev. B **50**, 17953–17979 (1994).
[37]H. Zheng, X. G. Li, R. Tran, C. Chen, M. Horton, D. Winston, K. A. Persson, and S. P. Ong, "Grain boundary properties of elemental metals," Acta Mater. **186**, 40–49 (2020).
[38]T. Frolov, W. Setyawan, R. J. Kurtz, J. Marian, A. R. Oganov, R. E. Rudd, and Q. Zhu, "Grain boundary phases in bcc metals," Nanoscale **10**, 8253–8268 (2018).
[39]T. Nishiyama, A. Seko, and I. Tanaka, "Application of machine learning potentials to predict grain boundary properties in fcc elemental metals," Phys. Rev. Mater. **4**, 123607 (2020).
[40]C. Li, S. Lu, and L. Vitos, "Predicting grain boundary energies of complex alloys from *ab initio* calculations," Scr. Mater. **203**, 114118 (2021).
[41]Data retrieved from the Materials Project for Au (mp-81) from database version v2023.11.1 (n.d.), see https://next-gen.materialsproject.org/materials/mp.
[42]X. Yao, Y. Mao, and Y. F. Guo, "Effects of alloying elements on the generalised stacking fault energies of Pt: A first-principles study," Philos. Mag. **101**, 1033–1047 (2021).
[43]X. Yao, Y. F. Guo, X. Z. Tang, K. Xiong, and Y. Mao, "First-principles study on the effects of the alloying elements on the structural stability and mechanical properties of γ-Pt/γ'-Pt3X (X = Al, Hf, Zr) interfaces," Appl. Surf. Sci. **605**, 154744 (2022).
[44]H. Okamoto and T. B. Massalski, "The Au-Pt (gold-platinum) system," Bull. Alloy Phase Diagrams **6**, 46–56 (1985).
[45]J. O. Andersson and J. Ågren, "Models for numerical treatment of multicomponent diffusion in simple phases," J. Appl. Phys. **72**, 1350–1355 (1992).
[46]M. Matsuura, T. Yokoi, Y. Ogura, and K. Matsunaga, "Anharmonicity in grain boundary energy for Al: Thermodynamic integration with artificial-neural-network potential," Scr. Mater. **236**, 115685 (2023).
[47]A. V. Ruban, H. L. Skriver, and J. K. Nørskov, "Surface segregation energies in transition-metal alloys," Phys. Rev. B **59**, 15990–16000 (1999).
[48]W. T. Geng, A. J. Freeman, and G. B. Olson, "Influence of alloying additions on grain boundary cohesion of transition metals: First-principles determination and its phenomenological extension," Phys. Rev. B **63**, 165415 (2001).
[49]A. Y. Lozovoi and A. T. Paxton, "Boron in copper: A perfect misfit in the bulk and cohesion enhancer at a grain boundary," Phys. Rev. B **77**, 165413 (2008).
[50]G. Rein, H. Mehrer, and K. Maier, "Diffusion of ^{197}Pt and ^{199}Au in Pt at low temperatures," Phys. Status Solidi A **45**, 253–261 (1978).
[51]L. Y. Tian, H. Levämäki, O. Eriksson, K. Kokko, Á. Nagy, E. K. Délczeg-Czirják, and L. Vitos, "Density functional theory description of the order-disorder transformation in Fe–Ni," Sci. Rep. **9**, 1–7 (2019).
[52]B. Million, "Diffusion processes in the Fe–Ni system," Mater. Sci. Eng. **50**, 43–52 (1981).